Science of Sintering, **51** (2019) 265-276

doi:https://doi.org/10.2298/SOS1903265T

UDK: 661.872.2; 548.73

Photocatalytic Degradation of Bisphenol A with α-Fe_2O_3 Fibers and Particles

Nataša Z. Tomić[1], Marija M. Vuksanović[1*)], Đorđe Veljović[2], Veljko Đokić[1], Aleksandar D. Marinković[2], Radmila Jančić Heinemann[2]

[1]Innovation center of Faculty of Technology and Metallurgy, Karnegijeva 4, 11070 Belgrade, Serbia

[2]University of Belgrade, Faculty of Technology and Metallurgy, Karnegijeva 4, 11070 Belgrade, Serbia

Abstract:

Two-step synthesis of Fe_2O_3 particles, performed by precipitation from iron(III) chloride ($FeCl_3$•$6H_2O$) using ammonium hydroxide in first step and calcination at 400 and 700 °C during 4 h, provided Fe_2O_3 400 °C and Fe_2O_3 700 °C photocatalysts, respectively. The electrospinning process was used to prepare iron oxide fibers, named Fe_2O_3 fiber. Morphological and structural properties of samples were determined by Scanning Electron Microscopy (SEM), X-ray diffraction (XRD), Fourier Transform Infra-Red (FT-IR) and BET/BJH analysis. It was found that the α-Fe_2O_3 phase (hematite) has shown the compaction of the structure at 700 °C, i.e. lower textural properties. Hematite particles and fibers are used for bisphenol A (BPA) removal by photocatalytic decomposition and the enhanced catalytic performance was found with the use of Fe_2O_3 400 °C particles.

Keywords*: Bisphenol A; Photocatalytic degradation; Electrospinning; α-Fe_2O_3; Precipitation method.*

1. Introduction

Iron oxide plays an important role in many geological and biological processes and represents a very important material due to its non-toxicity, low cost, catalytic activity, and biocompatibility. The most used iron oxides are FeO, Fe_2O_3, Fe_3O_4. Iron(III) oxide has four crystallographic phases: hematite (α- Fe_2O_3), β-Fe_2O_3, maghemit (γ-Fe_2O_3) and ε-Fe_2O_3 [1]. Among them, α- Fe_2O_3 is the most stable under ambient conditions and has a wide range of applications in catalysis, pigments, biomedical materials, lithium batteries, adsorbents, solar cells, etc. [2-6]. Different techniques may be used in the preparation of powdered hematite: hydrothermal technique [7], sol-gel method [8] and co-precipitation method [9, 10]. Among these techniques, for the preparation of powdered hematite, chemical precipitation is attractive due to low costs, high purity, short preparation time, homogeneous particle distribution and the ability to produce excellent polycrystalline samples.

Electrospinning is a simple method for producing nanofibers for various applications [11, 12]. α-Fe_2O_3 nanofibers may be obtained via a simple hydrothermal route or electrospinning process followed by calcination that may be used in the removal and recovery of noxious Cr(VI) from wastewater [13, 14]. Interconnected 1D hollow structure of α-Fe_2O_3

*) **Corresponding author:** mdimitrijevic09@gmail.com

nanofibers was made by annealing of electrospun poly(vinyl alcohol) (PVA)-Fe_3O_4 composite fibers and used in dye removal [15, 16].

Bisphenol A (BPA) has become a significant contaminant since three million tons of this compound are produced every year worldwide. It is used as a raw material for the preparation of epoxy and polycarbonate resins (eg coatings for water containers, baby bottles and medical devices). Due to its massive use, BPA contamination is found in all environmental protection sections, including air, water and soil [17]. Many recent research efforts have focused on the photocatalytic treatments for BPA removal [**Error! Bookmark not defined.**8, 8, 9]. In the context of environmental protection, iron-enriched clay catalysts even at lower activity have an advantage over homogeneous iron catalysts which can be further improved by increasing the iron content [18, 19]. In addition, the photocatalysts should be easily separable from the water, in order to improve the ease of recycling and reusing the photocatalysts [20].

The aim of this study was: (i) to explore the synthesis of hematite particles and fibers, and (ii) to test their catalytic activity as heterogeneous catalysts for Fenton degradation of BPA in aqueous solutions. Two different methods were used: precipitation followed by calcination at two different temperatures for the synthesis of α-Fe_2O_3 particles, i.e. Fe_2O_3 400 ^oC and Fe_2O_3 700 ^oC, and electrospinning for the synthesis of hematite fibers, i.e. Fe_2O_3 fiber. These heterogeneous catalysts were meant to enable not only academic significance but also industrial due to good photo-catalytic activity and enhanced feasibility of the Fenton process for the treatment of wastewaters.

2. Experimental Procedures

2.1. Materials

Iron(III) chloride ($FeCl_3 \cdot 6H_2O$) was purchased in the crystallized state from the Clariant company. Poly(vinyl alcohol) (PVA), trademark Mowiol 18 – 88 with M_w = 130.000 g/mol was purchased from Sigma Aldrich. Ammonium hydroxide (NH_4OH) was purchased from NRK INŽENjERING doo, Serbia. Hydrogen peroxide (H_2O_2) and Bisphenol A (BPA) was supplied from Sigma Aldrich. All the chemicals were used without further purification. Deionized water was used in all experiments.

2.2. Preparation of electrospun hematite fibers

The electrospinning procedure was used for the preparation of iron oxide ceramic fibers. The water solution of PVA/$FeCl_3 \cdot 6H_2O$ was made with a mass ratio of 1:1. The solution was stirred on the laboratory mixer for 3h, and subjected to electrospinning using Electrospinner CH – 01 (Linari Engineering, Italy). The solution was placed into the 20 mL plastic syringe having a needle of 0.8 cm orifice. The high voltage supply (Spelmann PCM50P120, USA) capable of producing the 30 kV was used in experiments. The precursor solutions were used in supplied to the nozzles using syringe pumps of the R100E type (Razel Scientific Instruments, USA). The voltage applied in experiments was ~28 kV. The mass flow varied around 0.05 mL/h, while the distance between the needle and the alumina foil collector was 15 cm. Obtained fibers were dried and then heat-treated at 700 ^oC during 2 h in air, and denoted as Fe_2O_3 fiber.

2.3. Preparation of Fe_2O_3 particles

Hematite particles were synthesized by the chemical precipitation method. An aqueous solution was prepared by dissolving 5 g $FeCl_3 \cdot 6H_2O$ in 100 mL of deionized water

under magnetic stirring for 30 min. An aqueous solution of 2M of NH_4OH (50 mL), used as the precipitating agent, was added gradually to maintain a pH value of 11. The resulting precipitations were collected and centrifuged at 6000 rpm, washed with distilled water and ethanol for several times and dried in air. Particles calcined at 400 ^oC and 700 ^oC for 4 h were denoted Fe_2O_3 400 ^oC and Fe_2O_3 700 ^oC, respectively.

2.4. Photocatalytic experiments

The photocatalytic performance of the synthesized catalyst samples was evaluated according to the rate of BPA degradation. A 300 W xenon lamp (PE300BF) was used as a light source. In a typical procedure, 10 mg of catalyst was suspended in 50 mL of BPA aqueous solution (C_0 = 20 mgL^{-1}, pH = 5.0), and the mixture was stirred for 30 min to reach an adsorption equilibrium. Aqueous solution H_2O_2 (1.0 mL, 1 %) was added to the reaction solution at the beginning of the irradiation. Then, the suspension was stirred in the dark for 30 min before the lamp was turned on. The concentration of BPA in the system was followed according to the peak at 276 nm by UV-Vis spectroscopy. It was found that the solution pH had no significant impact on photocatalysis, while the acidic conditions slightly reduced sorption capacity and hydrogen bonding between Fe_2O_3 and BPA [21].

2.5. Characterization methods

The morphology of the fibers and particles was examined using the FE-SEM, MIRA 3 TESCAN electron microscope operated at 20 kV. The image analysis tool (Image-Pro Plus 4.0, Media Cybernetics) was used to obtain the fiber and particles diameter distribution.

X-ray diffraction (XRD) patterns were recorded with an Ital Structure APD2000 X-ray diffractometer in a Bragg–Brentano geometry using CuKα radiation (λ = 1.5418 Å) and step-scan mode (range: 20−90° 2θ, step-time: 0.5 s, step-width: 0.02°).

The specific surface area and pore volume/size were measured using Micromeritics ASAP 2020 surface area and porosity analyzer. The samples were previously degassed under vacuum at 150 ^oC for 11 h.

The structural analysis of calcined powders synthesized at different temperatures was performed by single-beam Fourier-Transfer Infrared Spectroscopy (FTIR) using a Nicolet iS10 spectrometer (Thermo Scientific) in the attenuated total reflectance (ATR) mode with a single bounce 45 °F Golden Gate ATR accessory with a diamond crystal, and DTGS detector. FTIR spectra were obtained at 4 cm^{-1} resolution with ATR correction. The FTIR spectrometer was equipped with OMNIC software and recorded the spectra in the wavelength range from 2.5 μm to 20 μm (i.e., 4000-500 cm^{-1}).

The concentrations of the bisphenol A were determined using UV-Vis spectroscopy (Shimadzu UV-1800 spectrophotometer).

A laboratory pH meter, InoLab Cond 730 precision conductivity meter (WTW GmbH), with an accuracy of ± 0.01 pH units, was used for the pH measurements. The pH values at the point of zero charges (pH_{PZC}) were measured using the pH drift method [22].

3. Results and Discussion

3.1. The microstructure of the ferrous oxide based fibers and particles

In order to explain properly the photocatalytic activity of the crystalline materials, it is important to study morphology evolution (surface area, porosity, *etc.*). Morphology evolution is of particular importance because it may significantly modify physical properties and surface reactivity. The SEM micrographs of particles and electrospun fibers are shown in

Fig. 1. Fe_2O_3 400 ^oC (Fig. 1a) particles show somewhat higher surface roughness than Fe_2O_3 700 ^oC (Fig. 1b). Higher temperatures lead to the compaction of particles resulting in smooth microstructure and the occurrence of very fine particles that can be caused by the breaking off of larger particles due to compaction. A smooth surface of raw Fe_2O_3 fibers is noticed due to the presence of PVA in its structure. PVA degradation at 700 ^oC caused the formation of fibers porosity that can be of interest for the application in photocatalytic experiments.

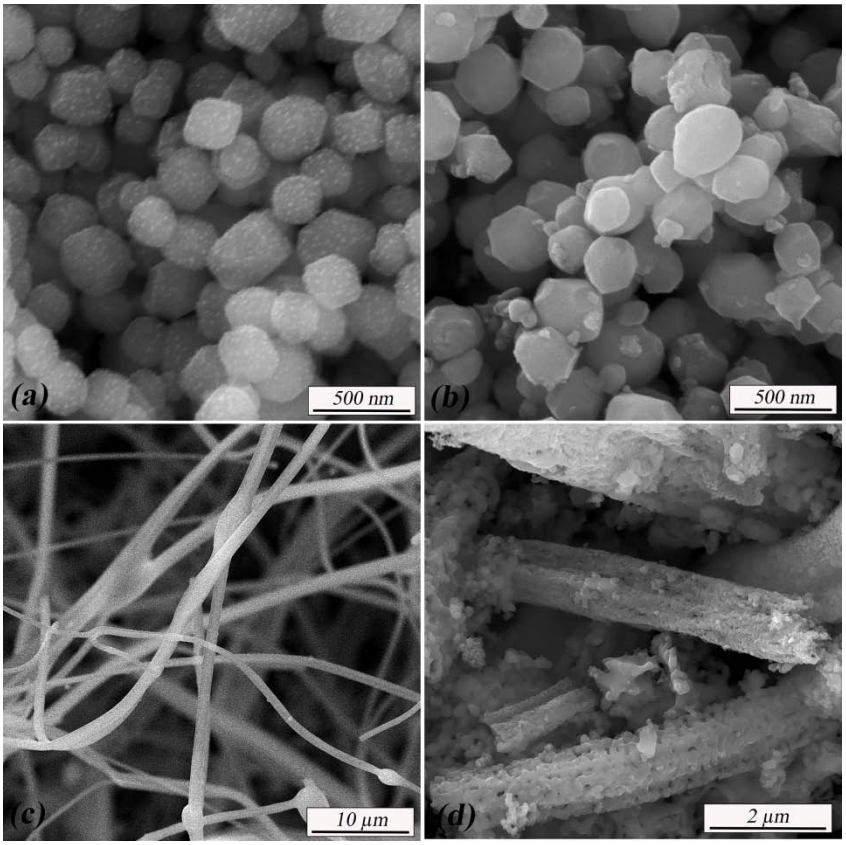

Fig. 1. The SEM micrographs: a) α – Fe_2O_3 particles at 400 ^oC, b) α – Fe_2O_3 particles at 700 ^oC, c) raw fiber obtained by the electrospinning method and d) fiber obtained by the electrospinning method at 700 ^oC.

These images were used to measure the diameters of α – Fe_2O_3 spherical particles and fibers obtained by the electrospinning method. The image analysis software (Image Pro Plus 6.0) was used to obtain the fiber and particles diameter distribution. Mean diameter distribution of α-Fe_2O_3 fibers and α-Fe_2O_3 particles calcined at 400 and 700 ^oC is shown in Fig. 2.

The mean diameters of the spherical α-Fe_2O_3 particles calcined at 400 ^oC and the α-Fe_2O_3 particles calcined at 700 ^oC were found to be 296.6 nm and 253.1 nm, respectively, according to results presented in Fig.s 2a and 2b. Accordingly, the calcination temperature increase affects the reduction of the particle diameter. The mean diameter of the raw fibers after calcination decreases from 1255 nm to 878 nm, Fig. 2c and 2d. Transformation to the well-defined crystal structure of particles leads to the collapse of the pores of the low-temperature generated phase and the consequent decrease of the particle specific surface area [19]. Compaction of α-Fe_2O_3 particles at higher temperatures leads to a decreased particles size.

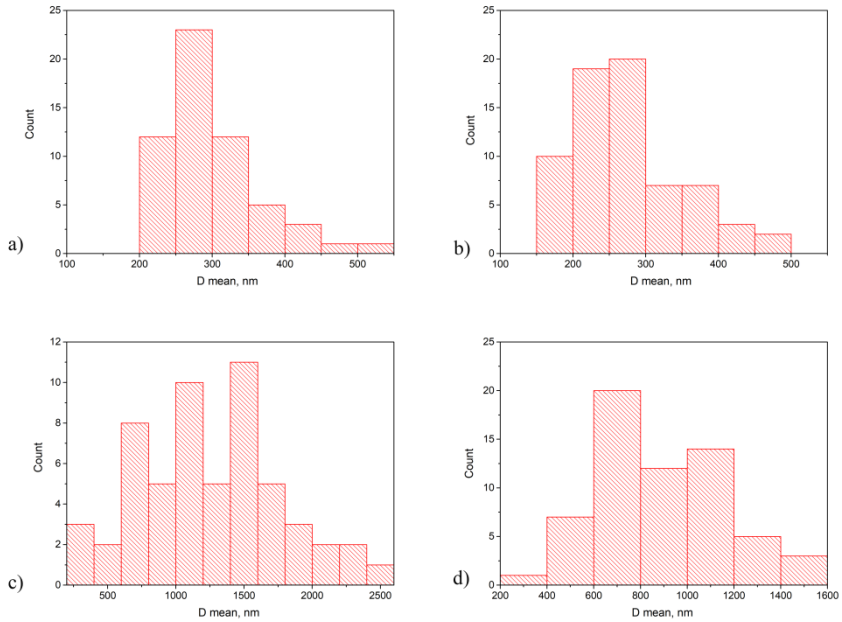

Fig. 2. Diameter distribution: a) α – Fe_2O_3 particles at 400 °C, b) α – Fe_2O_3 particles at 700 °C and c) raw fiber obtained by the electrospinning method and d) fiber obtained by the electrospinning method at 700 °C.

In order to obtain high adsorption of BPA and good photocatalytic activity, it is necessary to provide high availability of surface active sites at the particle/solution interfaces. Such behavior depends on the morphology of the catalyst, *i.e.*, particle size and surface area, as well as on particle interaction with BPA. Determined textural characteristics are presented in Table I. Larger pore volume, diameter and S_{BET} of α-Fe_2O_3 400 °C particles, in comparison to particles calcined at 700 °C, *i.e.* α-Fe_2O_3 700 °C, was found. These phenomena could be explained as the consequence of the structure densification as noticed by the decrease of particle diameter at the higher temperature of calcination. The electrospinning process enabled obtaining slightly higher S_{BET} than the α-Fe_2O_3 700 °C particles produced at the same calcination temperature. The significantly increased porosity of the α-Fe_2O_3 fiber was obtained as well.

Determined pH_{PZC} values for calcined particles at 400 and 700 °C was 4.9 and 5.1, respectively, while the pH_{PZC} of α-Fe_2O_3 fiber was found to be 5.0. Small differences in pH_{PZC} values indicate low influence of production technology/parameters on the surface properties of obtained materials. The pH of the point of zero charges, pH_{PZC}, is the pH value at which the surface concentrations of positive and negative charges/groups are equivalent. In aqueous systems, the surface of synthesized samples is covered with functional groups that can be protonated at pH values below pH_{PZC} or deprotonated at higher pH. Electrostatic and hydrogen bonding attractive/repulsive forces between BPA and surface charges are responsible for adsorption and photocatalytic activity. Such results indicate that irrespectively to used photocatalysts similar pH-dependent adsorption behavior could be expected, considering electrostatic interactions. Effective ionization of BPA could be expected at pH>8. In general, adsorption efficiency at operational pH significantly depends on hydrogen bonding of BPA hydroxyl groups with particles surface functionalities capable to participate in proton-donating/accepting interactions.

Tab. I Textural characteristics of α-Fe_2O_3 particles and fibers.

Parameter/Sample	α-Fe_2O_3 400 °C	α-Fe_2O_3 700 °C	α-Fe_2O_3 fiber
Specific surface area, S_{BET} (m^2 g^{-1})	13.050	2.788	5.642
Total pore volume, V_{total} (cm^3 g^{-1})	0.116	0.009	0.028
Mesopore volume, V_{meso} (cm^3 g^{-1})	0.114	0.009	0.021
Mean mesopore diameter, D_{mean} (nm)	28.819	13.708	15.174
pH_{PZC}	4.9	5.1	5.0

3.2. X-ray diffraction

The X-ray diffraction is used to identify the crystalline structure of obtained iron oxide structure. By the X-ray powder diffraction (XRPD) technique, the Fe_2O_3 was identified as a stable α-Fe_2O_3 (hematite) form (ICSD 161294 card) in all samples. The program PowderCell [23] was used for an approximate phase analysis. The mean crystallite size of α-Fe_2O_3 phase was estimated from the most intensive diffraction peaks by the program PowderCell.

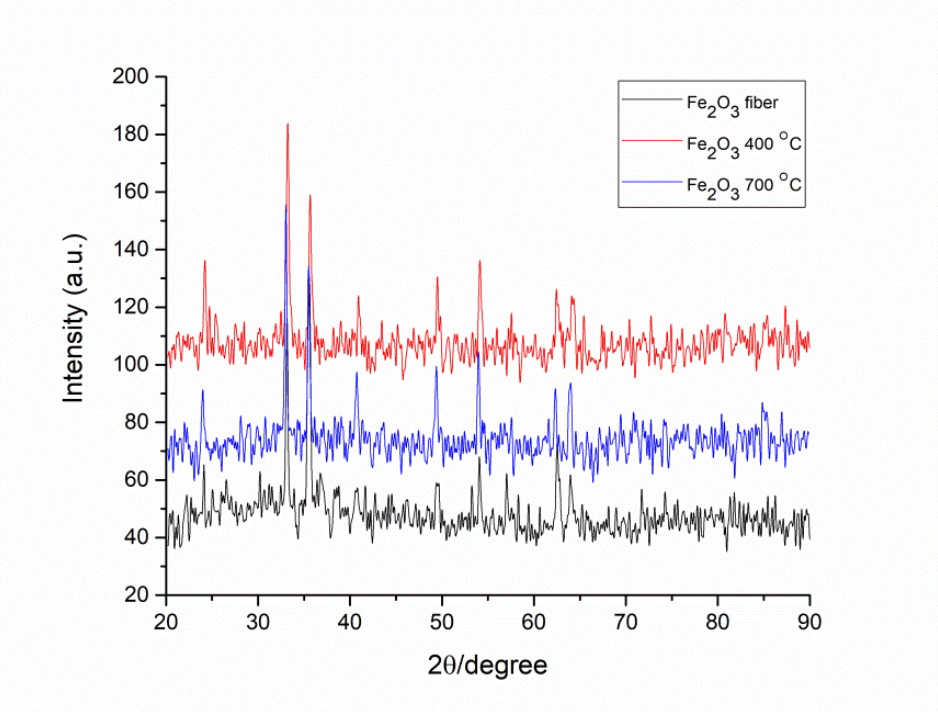

Fig. 3. XRD patterns of α-Fe_2O_3 phase observed in all samples.

The determined unit cell parameters of characterized samples are: α-Fe_2O_3 fiber: a = 5.0278, c = 13.6962 Å; α-Fe_2O_3 400 °C: a = 5.0331, c = 13.7431 Å; α-Fe_2O_3 700 °C: a = 5.0282, c = 13.7250 Å. Obtained value for the mean crystallite size of all samples was 34.4

nm. Also, noticed a slight decrease in lattice parameters proved the presumption about the structure densification at higher temperatures.

3.3. Fourier-Transfer Infrared Spectroscopy (FTIR)

The hematite composition was observed using Fourier Transform Infra-Red (FTIR) spectroscopy. The spectra of the title compounds were performed at room temperature between 4000 and 450 cm^{-1}. The FTIR spectral bands are shown in Fig. 4.

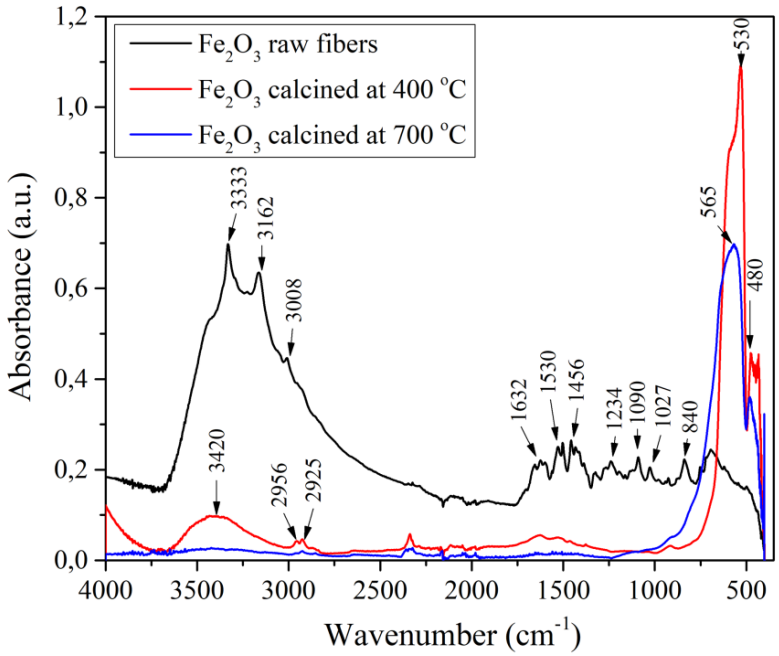

Fig. 4. FTIR spectra of raw fiber α-Fe_2O_3 before calcination, and α-Fe_2O_3 particles calcined at 400 and 700 °C.

A spectrum of raw Fe_2O_3 fibers shows broad characteristic peaks at 3162 to 3333 cm^{-1} and peak at 1632 cm^{-1} attributed to the -OH stretching and bending vibration of PVA, respectively [8, 24]. In the same wavelength region, Fe_2O_3 400 °C particles show the absorption of at 3420 cm^{-1} that originates from Fe_2O_3 surface OH groups. The peak at 2925 and 2956 cm^{-1} corresponds to the C–H stretching of $–CH_2$ groups [25]. There is a peak at 1456 cm^{-1} assigned to the deformation of CH_3 group [2]. For the calcined hematite synthesized by the precipitation method, the strong absorption peaks at 480, 530 and 565 cm^{-1} can be attributed to the Fe–O band vibrations [26, 27].

3.4. BPA removal

An index of the propensity of a metal oxide surface to ionize as a function of pH is the value of required pH to give zero net surface charge, denoted as pH_{PZC}. A variation of pH_{PZC} was observed in relation to applied calcination temperature (Table I). It was found that the nature and the surface area of metal oxides determine the pH_{PZC} value [26]. Low difference between the Fe_2O_3 400 °C and Fe_2O_3 700 °C may be a consequence of similar crystal structure and a difference in surface area, i.e. 13.050 and 2.788 m^2/g, respectively. Similar stands for Fe_2O_3 fibers. Applied thermal treatment for α-Fe_2O_3 700 °C cause contraction in particle diameter and a decrease in pore diameter, which in turn cause a slight

increase in pH_{PZC}. Change in pH_{PZC} reflects a change in a ration of ionizable surface groups but not their quantitative value. This aspect of photocatalyst surface properties significantly influences BPA absorptivity as one of a prerequisite for the achievement of effective photocatalytic reaction with generated active oxygen species at particles surface.

On the other hand, photocatalytic efficiency is also determined by an effective hole/electron separation induced by photon absorption. Their subsequent transport to photocatalyst surface and participation in the reaction of holes and surface-bound water and/or hydroxyl groups, i.e. time-dependent production of the most active oxidative species (the hydroxyl radical – $OH^{\bullet}$) determine photocatalytic efficiency. If photo-excited electrons and holes are trapped at crystal facets, and subsequent surface transfer of electrons/holes (initiation of surface reaction) occurs efficiently, such processes would minimize possible recombination, which causes a decrease of photocatalytic efficiency.

Fig. 5 represents the efficiency of α-Fe_2O_3 particles and fibers for BPA removal used as catalysts under UV light. Presented results suggest that the dense surface morphology of α-Fe_2O_3 700 ^oC particles contribute to the decrease of catalytic activity. Calcination at lower temperatures produces particles with the looser structure which gives α-Fe_2O_3 400 ^oC particles 40 % higher efficiency for BPA removal than α-Fe_2O_3 700 ^oC particles. An interesting phenomenon is noticed for α-Fe_2O_3 fibers. Their higher efficiency was superior for 34.4 % compared to α-Fe_2O_3 700 ^oC particles, this may be prescribed to the porous surface morphology (Fig. 1) due to the PVA removal. These results suggest that the simple method at lower temperatures for obtaining α-Fe_2O_3 particles may be used for BPA removal whose efficiency is almost identical to α-Fe_2O_3 fibers obtained by more demanding process.

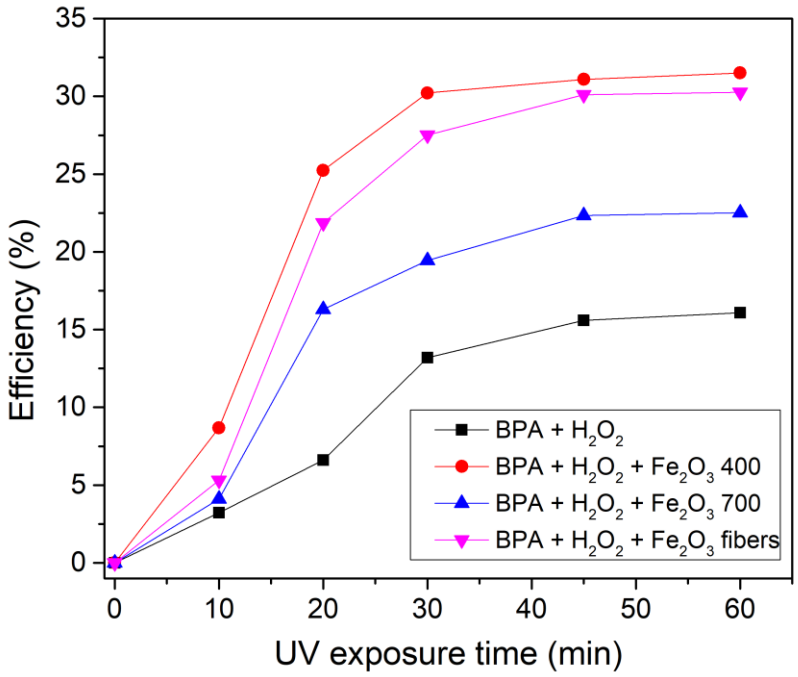

Fig. 5. The efficiency of BPA removal by UV light and photocatalytic degradation using synthesized catalysts.

BPA degradation has been found to be predominantly achieved *via* direct oxidation as well due to $OH^{\bullet}$ oxidation which are the major oxidants that degrade BPA [20, 1]. The most possible pathways are presented in Fig. 6.

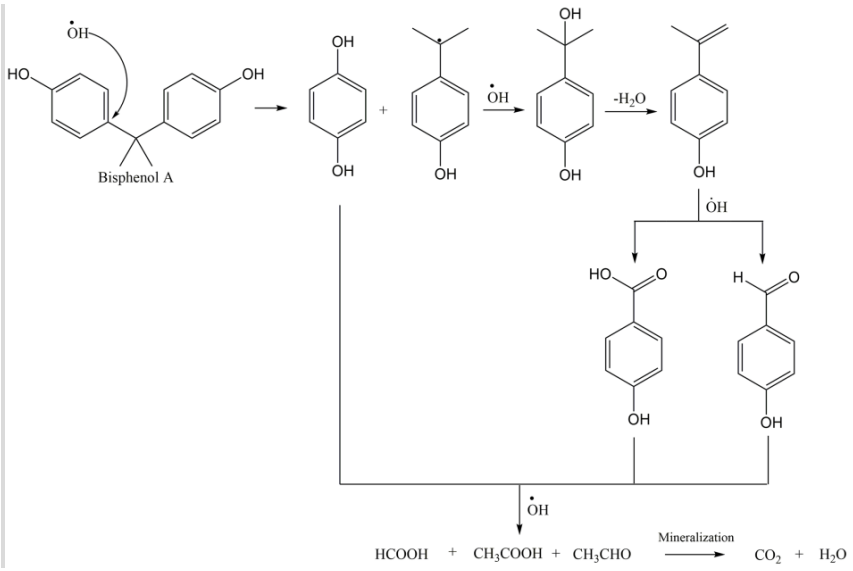

Fig. 6. Proposed mechanism of OH• radical mediated photocatalytic degradation of BPA [20].

Complete mineralization of BPA, as the main goal of the photocatalytic study, could be achieved using Fenton or Photo-Fenton processes, and fragmentation paths lead through mostly acidic species. As an evidence of suggested processes pH decreases from initial pH of 5 to 4.4 which clearly evidenced generation of acidic fragments/structure.

3.5. Comparative analysis of the catalytic performance of α-Fe_2O_3 and other catalysts

The efficacy of studied materials is compared with the efficacy of other catalysts used for BPA removal and it is presented as comparative results in Table II. There is a lack of information in the literature on photocatalytic properties of Fe_2O_3 particles and fibers. Table II compares the photodegradation efficiency of BPA using the iron oxide prepared in this work with the iron oxide based catalyst and others similar ones.

Tab. II Comparison of degradation efficiency of α-Fe_2O_3 obtained from this study and other photocatalysts.

Catalyst	Irradiation duration (min)	Dosage	Efficiency (%)	Reference
Ferrihydrite/PAC	360 60	1000 mg/L	58 ~30	[30]
Magnetite/PAC	360 60	1000 mg/L	50 ~20	[30]
Hematite/PAC	360 60	1000 mg/L	42 ~15	[30]
ZnO	360 60	5000 mg/L (0.5 w/v %)	99 ~17	[31]
Fe_2O_3	390	5000 mg/L (0.5 w/v %)	80	[31]
TiO_2 degussa P25	60	5000 mg/L (0.5 w/v %)	98	[32]
TiO_2	80	10 mg/L	97	[33]
Fe_2O_3 400 ºC	60	20 mg/L	33	this work

In the literature, the researcher sometimes used longer times for photocatalysis (i.e. 360, 390 min). Since the most efficient time of catalysis in this work was 60 min, Table 2 also provides the extracted values of photocatalytic efficiency at 60 min from literature charts. According to the presented values for 60 min of catalysis, Fe_2O_3 400 ^oC particles showed higher efficiency than other iron oxide based catalysts even at much lower dosage. The best photocatalytic performances of TiO_2 property for the removal of BPA are obvious according to Table II.

4. Conclusion

In this study, iron oxide (α-Fe_2O_3) particles were prepared with precipitation method. The particles were calcined at 400 and 700 ^oC and average diameter for particles were 296.6 nm and 253.1 nm, respectively. Iron(III) chloride/PVA fibers were obtained using the electrospinning method. The calcination was done at 700 ^oC and the fibers had 878 nm average diameter. XRD, BET, SEM, FT-IR and UV-Vis techniques were used to characterize the synthesized samples. The synthesized samples are used for the removal of Bisphenol A by photocatalytic decomposition. The removal efficiency of α-Fe_2O_3 400 ^oC particles is significantly higher (for 40 %) than the efficiency of α-Fe_2O_3 700 ^oC particles due to more loosely surface morphology obtained at lower calcination temperatures. In addition, a high catalytic activity may be obtained at higher temperatures (700 ^oC) using the electrospinning process whereby α-Fe_2O_3 fibers showed 34.4 % higher catalytic activity then α-Fe_2O_3 700 ^oC.

Acknowledgments

This research has been financed by the Ministry of Education, Science and Technological Development of the Republic of Serbia as a part of the project TR34011.

5. References

1. S. Sakurai, A. Namai, K. Hashimoto, S. I. Ohkoshi, Am. Chem. Soc., 131 (2009) 18299.
2. M. M. Khadar, N. N. Lichtin, G. H. Vurnes, M. Salmenon, G. A. Somoraj, Langmuir, 3 (1987) 303.
3. J. Shakhpure, H. Vijayanand, S. Basavaraja, V. Hiremath, A. Venkatraman, Bull. Mater. Sci., 28 (2005) 713.
4. M. Tadic, N. Citakovic, M. Panjan, Z. Stojanovic, D. Markovic, V. Spasojevic, Alloy. Comp., 509 (2011) 7639.
5. J. Chen, L. N. Xu, W. Y. Li, X. L. Gou, Adv Mater., 17 (2005) 582.
6. X. Zhu, Y. Zhu, S. Murali, M. D. Stoller, R. S. Ruoff, ACS Nano., 5 (2011) 3333.
7. A. Lassoued, M. S. Lassoued, B. Dkhil, S. Ammar, A. Gadri, Phys. E Low-dimens. Syst. Nanostruct., 101 (2018) 212.
8. M. I. B. Bernardi, S. Cava, C. O. Paiva-Santos, E. R. Leite, C. A. Paskocimas, E. Longo, J. Eur. Ceram. Soc., 22 (2002) 2911.
9. A. Lassoued, M. S. Lassoued, B. Dkhil, S. Ammar, A. Gadri, Phys. E Low-dimens. Syst. Nanostruct. 97 (2018) 328.
10. A. Lassoued, B. Dkhil, A. Gadri, S. Ammar, Res. Phys. 7 (2017) 3007.
11. P. Milanović, M. Dimitrijević, R. Jančić Heinemann, J. Rogan, D. B. Stojanović, A. Kojović, R. Aleksić, Ceram. Int., 39 (2013) 2131.

12. P. Milanovic, M. Vuksanovic, M. Mitric, D. Stojanovic, A. Kojovic, J. Rogan, R. Jancic – Hainemann, Sci. Sinter., 50 (2018) 77.
13. Y. Zhu, J. C. Zhang, J. Zhai, L. Jiang, Thin Solid Films., 510 (2006) 271.
14. T. Ren, P. He, W. Niu, Y. Wu, L. Ai, X. Gou, Environ Sci Pollut Res., 20 (2013) 155.
15. Q. Gao, J. Luo, X. Wang, C. Gao, M. Ge, Nanoscale. Res.Lett., 10 (2015) 176.
16. P. Milanović, M. M. Vuksanović, M. Mitrić, A. Kojović, D. Mijin, R. Jančić-Hainemann, Sci. Sinter., 50 (2018) 467-476.
17. P. Fu, K. Kawamura, Environ. Pollut., 158 (2010) 3138.
18. E. E. Kiss, J. G. Ranogajec, R. P. Marinković-Nedučin, T. J. Vulić, React Kinet Catal Lett., 80 (2003) 255.
19. E. E. Kiss, M. M. Lazic, G. C. Boskovic, React Kinet Catal Lett., 83 (2004) 221.
20. P. V. L. Reddy, K.-H. Kim, B. Kavitha, V. Kumar, N. Raza, S. Kalagara, J Environ Manage., 213 (2018) 189.
21. H. Park, J. R. Kodurua, K. Chooa, B. Lee, Journal of Hazardous Materials 286 (2015) 315.
22. D. Budimirović, Z. S. Veličković, V. R. Djokić, M. Milosavljević, J. Markovski, S. Lević, A.D. Marinković, Chem. Eng. Res. Des., 119 (2017) 75.
23. G. Lazouzi, M. M. Vuksanović, N. Z. Tomić, M. Mitrić, M. Petrović, V.Radojević, R. Jančić Hainemann, Ceram. Int., 44 (2018) 7442.
24. W. Kraus, G. Nolze, PowderCell for Windows, V.2.4, Federal Institute for Materials Research and Testing, Berlin, Germany, 2000.
25. Q. Gao, J. Takizawa, M. Kimura, Polymer., 54 (2013) 120.
26. L. J. Preston, M. R. M. Izawa, N. R. Banerjee, Astrobiology., 11 (2011) 585.
27. H. Liu, P. Li, B. Lu, Y. Wei, Y. Sun, Solid. State. Chem., 182 (2009) 1767.
28. A. Lassoued, M. S. Lassoued, B. Dkhil, A. Gadri, S. Ammar, Mol. Struct., 1148 (2017) 276.
29. S. S. Subramanian, J. S. Noh, J.A. Schwarz, J. Catal., 114 (1988) 433.
30. V. Repousi, A. Petala, Z. Frontistis, M. Antonopoulou, I. Konstantinou, D. I. Kondarides, D. Mantzavinos, Catal Today, 284 (2017) 59.
31. Y.-H. Tan, P.S. Goh, A.F. Ismail, Int Biodeterior Biodegradation., 102 (2015) 346.
32. W.-T. Tsai, M.-K. Lee, T.-Y. Su, Y.-M. Chang, J Hazard Mater., 168 (2009) 269.
33. C. Jia, Y. Wang, C. Zhang, Q. Qin, S. Kong, S. K. Yao, Environ. Eng. Sci., 29 (7) (2012) 630.

Садржај: *Двостепена синтеза Fe_2O_3 честица, изведена је таложењем из раствора гвожђе (III) хлорида ($FeCl_3$•$6H_2O$) коришћењем амонијум хидроксида у првом кораку и калцинације на 400 и 700 ^oC током 4 часа, и означени су као Fe_2O_3 400 ^oC и Fe_2O_3 700 ^oC, датим редом. Процес електропредења коришћен је за припрему влакана гвожђе оксида који су означени са α -Fe_2O_3 fiber. Морфолошка и структурна својства узорака одређена су Скенирајућом електронском микроскопијом, Рендгенском дифракцијом, Фуријеовом Трансформацијом Инфрацрвене Спектрометрије (ФТИР) и БЕТ/БЈХ анализом. Утврђено је да јеα -Fe_2O_3 фаза (хематит) показала контакцију структуре на 700 ^oC, тј. смањену порозност. Честице и влакна гвожђе оксида користе се за уклањање Бисфенола А фотокаталитичком декомпозицијом, а најбоља каталитичка својства показале су α-Fe_2O_3 400 ^oC честице.*

Кључне речи*: Бисфенол А, фотокаталитичка деградација, електропредење, α- Fe_2O_3, метода таложења.*